

**Experimental and theoretical investigation of optical properties of dysprosium monopnictides**

J. Schoenes

*Institut für Halbleiterphysik und Optik, Technische Universität Braunschweig, D-38106 Braunschweig, Germany*

P. Repond and F. Hulliger

*Laboratorium für Festkörperphysik, ETH Zürich, CH-8093 Zürich, Switzerland*

D. B. Ghosh and S. K. De

*Department of Materials Science, Indian Association for the Cultivation of Science, Jadavpur, Calcutta 700 032, India*

J. Kuneš

*Institute of Physics, Academy of Sciences, Cukrovarnická 10, CZ-162 53 Prague, Czech Republic*

P. M. Oppeneer

*Leibniz-Institute of Solid State and Materials Research, P.O. Box 270016, D-01171 Dresden, Germany*

(Received 3 March 2003; published 5 August 2003)

The electronic and optical properties of DyP and DyBi are investigated both experimentally and computationally. The reflectivity spectra, which have been measured up to 12 eV on single crystals, display richly peaked spectral structures that are analogous for both pnictides. From the measured reflectivities the plasma frequencies, Drude relaxation times, and optical conductivity spectra are derived. The fitted Drude conductivity reveals that DyP and DyBi are semimetals with a number of free carriers of about 0.16 and 0.23 per formula unit, respectively. The very-structured experimental optical conductivity spectra are compared to calculated spectra, which are computed using two different approaches to the Dy  $4f$  states: the open-core approach and the L(S)DA+ $U$  approach in three versions. These approaches to the  $4f$  states lead to very similar optical spectra. There exists a reasonable agreement between calculation and experiment for a number of the spectral features, which are interpreted by specific interband transitions within the calculated band structure. The agreement between theory and experiment substantiates that the  $4f$  electrons do not participate in the bonding. The differences that remain between theory and experiment for some of the spectral features do not appear to rest on aspects of the treatment of the  $4f$  states, but rather to be intrinsic shortcomings in the description of the other band states.

DOI: 10.1103/PhysRevB.68.085102

PACS number(s): 78.20.-e, 71.20.-b, 71.28.+d

**I. INTRODUCTION**

The rare-earth monopnictides have been the subject of investigations since the 1960s. These monopnictides have continued to attract considerable attention because of their numerous intricate magnetic, optical, and magneto-optical properties that were discovered.<sup>1-5</sup> Particular monopnictides that exhibit unusual properties are, e.g., the Ce and Yb monopnictides. CeP and CeSb were found to have extraordinarily rich magnetic phase diagrams.<sup>1,5</sup> CeAs, CeSb, and CeBi were reported to display an unusually large magneto-optical Kerr rotation.<sup>3,4</sup> Optical spectroscopy could prove that GdP is metallic, with a small number of free carriers derived from the Drude-type conductivity.<sup>6</sup> Similar metallic-like optical spectra were subsequently reported for a number of other rare-earth monopnictides, such as, e.g., LaSb, CeSb, PrSb, YbAs, and CeBi.<sup>7-12</sup> Very small Fermi surface areas were confirmed by de Haas-van Alphen measurements for several pnictides, such as, e.g., LaAs, GdAs, CeAs, and CeSb.<sup>13-15</sup>

The rare-earth monopnictides crystallize in the NaCl-type structure, with the exception of Eu which does not form monopnictides. In spite of such simple crystal structure, the electronic structure of the monopnictides has been a topic of

debate for years. Much of this debate is connected to the role that the  $4f$  electrons play in the electronic properties. In most rare-earth compounds, the  $4f$ 's are believed to be localized; however, the magnetic  $4f$ 's are exchange coupled to the  $5d$  conduction electrons near the Fermi energy. Itinerant  $4f$  behavior—or tendencies towards itinerant  $4f$  behavior—has been observed in CeN and CeP and in some of the Yb monopnictides. *Ab initio* calculations<sup>16</sup> of the optical spectrum of CeN, based on the assumption of itinerant  $4f$ 's, could fully reproduce the experimental optical spectrum.<sup>17</sup> For CeP, angular-resolved photoemission revealed a narrow, quasiparticle  $4f$  band just below the Fermi energy.<sup>18</sup> Also, the optical spectra of YbN and YbP were interpreted in terms of an unoccupied  $4f$  state being closely above the Fermi energy.<sup>19</sup>

On the theoretical side, the exact treatment of  $f$  electrons in rare-earth and actinide materials is still a complicated issue. The  $f$  electrons are strongly correlated and simultaneously influenced by the chemical environment as well as external conditions such as pressure. In the case of light rare-earth materials the  $4f$  delocalization can be appreciable and a  $f$  band formalism, based on the local spin density approximation (LSDA), gives consequently a good explanation of most experiments. For many other rare-earth materials the  $4f$

states are localized and hybridize only weakly with other valence states. In such cases, a viable description can be the open-core or pseudocore approach, in which the occupied  $f$  electrons are considered in a separate valence panel (see, e.g., Ref. 20). For example, the electronic and magnetic properties for the heavier rare-earth elements Gd and Tb are reasonably explained by the open-core description.<sup>21</sup> It was also used for the calculation of ground-state properties of Gd and Er based monpnictides.<sup>22</sup> A second approach to localized or semilocalized  $4f$  states is the LDA+ $U$  or LSDA+ $U$  method.<sup>23–26</sup> These approaches have been applied in the past to several rare-earth monpnictides with reasonable success.<sup>27–31</sup> A third approach to localized  $4f$  electrons that deserves to be mentioned, is the self-interaction-corrected (SIC) LSDA scheme, which has been used to compute the valencies and possible valence transitions of various rare-earth pnictides.<sup>32</sup>

In this work we report a combined experimental-theoretical investigation of the electronic structure and optical properties of DyP and DyBi. The electronic structure of the Dy monpnictides has not yet been investigated in detail (cf. Ref. 33). An infrared absorption study of DySb, addressing the number of carriers, was reported previously.<sup>34</sup> One of our aims is to ascribe the peaks in the measured optical conductivity spectra to particular interband transitions. A further aim is to address the differences that exist between the open-core and LSDA+ $U$  approaches to the localized  $4f$  electrons, which are so far only poorly investigated. A further, main purpose of this work is to elucidate the precise behavior of the Dy  $4f$  electrons both from experiment and first-principles electronic structure calculations.

## II. EXPERIMENTAL PROCEDURE

For the preparation of the single crystals of the two materials two different methods were used. A two-step process was used for DyP. In the first step, about 20 g DyP was prepared in powder form by reacting very fine 99.9% Dy turnings with 99.99% red phosphorus in evacuated closed silica tubes. Within several days the temperature was raised to 600 °C and kept there for some days. A final homogenization was carried out at 800 °C. The resulting powder was compacted into two pellets of 12 mm diameter and 10 mm height which both were enclosed under vacuum in a sealed tungsten crucible. The material was first melted, slowly cooled through the melting point, and then annealed 1 week at 20–40 K below the melting point.

The DyBi sample was prepared in a one-step process. Here 99.9% Dy turnings and 99.99% bismuth pieces of 17 g total weight were enclosed in an evacuated tantalum tube and slowly heated until a strongly exothermic reaction set in. After complete melting, the tube was cooled down and reversed. The ingot was then remelted and annealed for 15 min slightly below the melting temperature and subsequently cooled to room temperature. On opening the tantalum tube the ingot split into ashlarlike pieces of several mm length.

The optical reflectivity has been measured at room temperature in the energy range from 0.03 to 12 eV. To cover this range three different spectrometers had to be used. De-

tails of the two spectrometers covering the ranges 0.5–5 eV and 4–12 eV can be found in Ref. 35. For the far-infrared region (0.03–0.5 eV) an inset was constructed, allowing us also to cleave the crystal in this measurement chamber in a vacuum of  $10^{-5}$ – $10^{-6}$  Torr. The general procedure consists in first cleaving a crystal of a given material in the 0.5–5 eV spectrometer, which has an ultrahigh-vacuum sample chamber which allows reaching a pressure in the  $10^{-10}$  Torr range; then, after an immediate-reflectivity measurement, the measurement is repeated after several hours under the same vacuum conditions. Subsequently the pressure is increased to  $10^{-5}$  Torr, and the measurement is repeated a few times. Finally, the vacuum is broken and the measurement is repeated under atmospheric conditions. For DyP no changes were observed between the various spectra, and therefore the very same crystals were transferred to the two other spectrometers to determine the reflectivity in the respective spectral ranges. This procedure has the advantage of eliminating sample-dependent effects. For DyBi the various measurements in the 0.5–5 eV range showed good reproducibility as long as the vacuum was better than  $10^{-5}$  Torr, but a dramatic decrease of the reflectivity occurred when the crystals were kept in air for 30 min, indicating an oxidation of the surface. On inspection by eye, one could follow the disappearance of the metallic luster. This deterioration problem required that for every spectrometer new crystals be cleaved and the measurements performed *in situ*. Smaller deviations between the three different parts of the spectra have been corrected to eliminate spurious effects in the Kramers-Kronig transformation. For the latter the reflectivity curves were extrapolated to zero photon energy using the Hagen-Rubens relation with resistivity values determined in four-point van der Pauw measurements.

## III. THEORY

The electronic properties are calculated employing the full-potential linear-augmented-plane-wave (FLAPW) method as implemented in the WIEN2K package.<sup>36</sup> In this method, the unit cell is divided into two regions: nonoverlapping muffin-tin spheres around each atomic site and the interstitial region. Inside a muffin-tin sphere the basis functions are constructed as a linear combination of radial solutions of the Kohn-Sham equation and its energy derivative at a particular energy which is chosen at center of respective bands. A plane-wave expansion is used in the interstitial part. The maximum angular momentum quantum number is 10 for the expansion of wave functions inside the muffin-tin sphere. Cubic harmonics up to order 4 are used in the charge density and crystal potential for the construction of the full potential. The LSDA to the exchange-correlation potential in the parametrization according to Perdew and Wang<sup>37</sup> is used in our calculations. The spin-orbit interaction is taken into account in a second variation in each self-consistent loop.<sup>38</sup> For Dy in DyP and DyBi, the used muffin-tin radii  $R_{MT}$  are 2.60 and 3.00 a.u., respectively. The muffin-tin radii used for the pnictogen are 2.40 a.u. (P) and 2.85 a.u. (Bi), corresponding to the experimental lattice constants of 5.63 Å and 6.24 Å for DyP and DyBi. The number of basis functions is determined

by the relation  $R_{MT}K_{\max}=8.0$ . For Dy, the  $5s$ ,  $5p$ ,  $5d$ , and  $6s$  states and, for the pnictogen,  $s$ ,  $p$ , and  $d$  valence states were included in the valence panel.

In order to investigate in detail the role of the Dy  $4f$  states, we used two different methods for the treatment of the  $4f$  electrons: the open-core approach (see, e.g., Refs. 20 and 21) and the L(S)DA+ $U$  scheme in three variants.<sup>23–25</sup> These methods lead to an electronic structure in which basically the  $4f$  electrons are well below the Fermi energy ( $E_F$ ). The main differences rest in the unoccupied  $4f$  states (which are not present in the open-core approach) and in the occurrence of  $4f$  spin polarization. In the open-core approach, we consider for Dy a trivalent, nonmagnetic  $4f^9$  configuration, which is treated in a separate energy valence panel and its charge density contribution is added to the total density in each iteration. In case of the L(S)DA+ $U$  approaches, one has to deal with the fact that the  $4f$ 's spin polarize, leading to a local magnetic moment on Dy. These local moments are disordered under the adopted conditions of the experiment, however. In order not to complicate the treatment of the magnetic ordering too much, we assumed ferromagnetic order. As initial data for the L(S)DA+ $U$  calculations, we used the Dy  $4f$  occupation number matrix obtained from the open-core calculation. The values of the  $U$  and  $J$  parameters were chosen to be  $U=6.7$  eV,  $J=0.7$  eV, like those reported previously for Gd.<sup>39</sup> In the iterations, the occupation as well as the spin and orbital moments of the Dy  $4f$  was found to be preserved at the atomic values dictated by Hund's rules. The unoccupied  $4f$ 's were approximately 1 eV above the Fermi energy. To investigate if possible differences are connected with the available L(S)DA+ $U$  schemes, we performed test calculations with the two L(S)DA+ $U$  schemes<sup>24,25</sup> and with the LDA+ $U$  scheme.<sup>23</sup> In the latter scheme, spin polarization arises only due to the  $U$  term, while the crystal potential is unpolarized. Therefore, the polarization of the valence states is due to hybridization with the  $4f$ 's only. All L(S)DA+ $U$  calculations were performed in the rotationally invariant formulation.<sup>26</sup>

## IV. RESULTS

### A. Experimental results

Figure 1 shows the near-normal incidence reflectivity spectra for DyP and DyBi. We observe a metallic behavior at low frequencies, a reflectivity as high as 40% in the visible range, a number of well-resolved peaks and shoulders (labeled 1–9), and a decrease of the reflectivity toward the high-energy end of the spectra. On comparing the spectrum of DyP with those obtained previously on polished samples of GdP (Refs. 40 and 41) and DyP (Ref. 42) we observe that the present reflectivity is 10% (absolute value) higher in the visible range, about 15% higher at 9 eV and in addition much more structured. The differences between our DyBi spectrum and previous results for GdBi (Ref. 42) are even more striking, as the latter did not show a plasma minimum, but instead a nearly constant reflectivity of 12% between 5 and 12 eV. The present data of DyBi, which display the same number and type of structures as those observed for DyP, provide

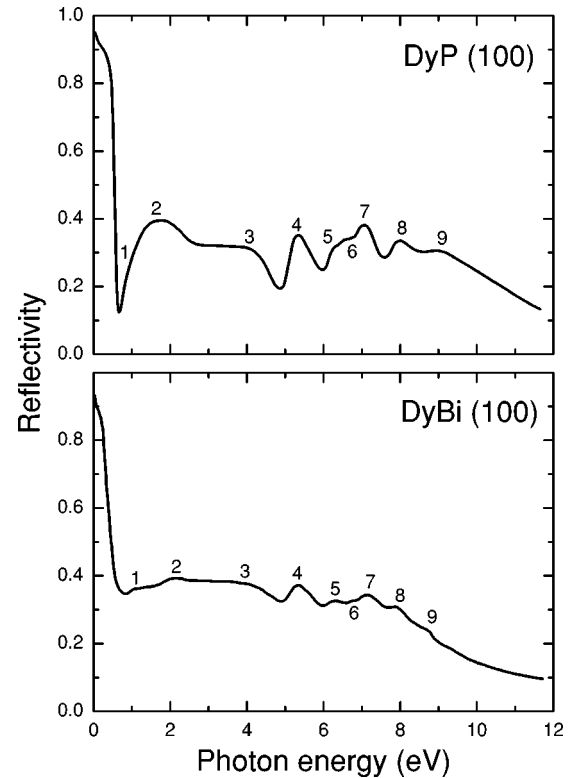


FIG. 1. Measured near-normal reflectivity spectra of DyP (top) and DyBi (bottom). The numbers label the fine structures in the spectra.

strong evidence that this spectrum is intrinsic for DyBi and is not falsified by oxidation or other surface and material problems.

The Kramers-Kronig transformation of the reflectivity spectra allows us to compute the complex dielectric function  $\varepsilon(\omega)$  ( $\equiv\varepsilon_1+i\varepsilon_2$ ), the complex optical conductivity  $\sigma(\omega)$  ( $\equiv\sigma_1+i\sigma_2$ ), the complex refractive index  $n=\sqrt{\varepsilon}$ , the energy-loss function  $\text{Im}[-\varepsilon^{-1}]$ , and the effective number of electrons,  $n_{\text{eff}}=m/(2\pi^2e^2N_m)\int_0^{\omega_{\max}}\omega\text{Im}\varepsilon(\omega)d\omega$ , which contribute to optical transitions up to the frequency  $\omega_{\max}$ . Here  $m$  is the electron mass and  $N_m$  is the number of formula units (molecules) per  $\text{cm}^3$ . For sake of brevity, we will not discuss all these optical functions; in particular we shall omit the refractive index and dielectric function, and we shall postpone discussing the optical conductivity to Sec. IV B, where we compare theoretical and experimental results. DyP and DyBi are cubic materials, yet the antiferromagnetic ordering could impart some departure from strict cubic symmetry. However, the magnetic ordering temperatures for DyP and DyBi are 8 K and 13 K, respectively, whereas the optical measurements have been performed at room temperature, and the optical properties can thus be considered isotropic. The  $f$ -electron cubic crystal-field splitting is very small on the energy scale of the optical excitation and so is not included in our analysis. The resistivity values used for the extrapolation of the reflectivity to zero energy in the Hagen-Rubens relation  $R=1-2\sqrt{\rho_0\omega/2\pi}$  have been determined as  $\rho_0=(63\pm 3)\mu\Omega\text{ cm}$  in DyP and  $\rho_0=(86\pm 5)\mu\Omega\text{ cm}$  in DyBi.

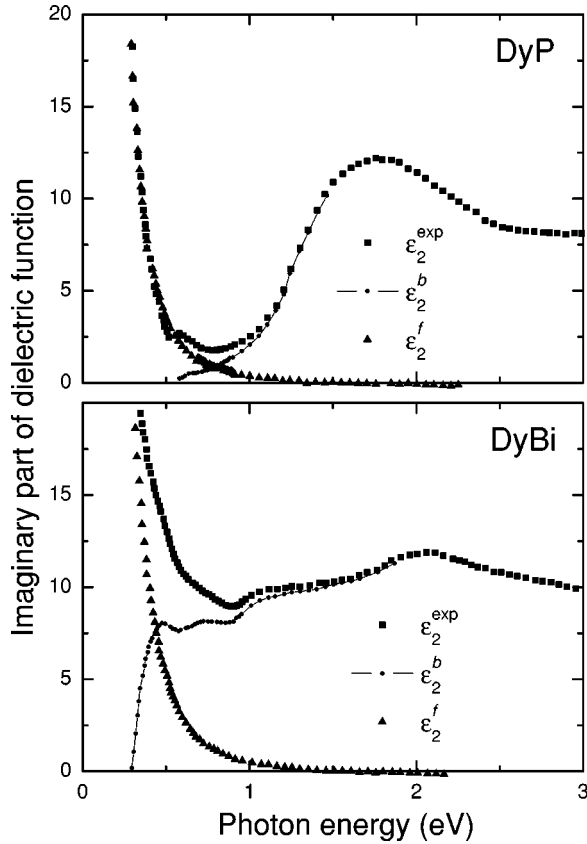


FIG. 2. Decomposition of the imaginary part of the dielectric function ( $\epsilon_2^{\text{exp}}$ ) into the free-electron ( $\epsilon_2^f$ ) and interband ( $\epsilon_2^b$ ) contributions for DyP (top) and DyBi (bottom).

The full dielectric functions  $\epsilon(\omega)$  derived from the reflectivity spectra are not shown here, but we mention that its low-energy behavior appears free electron like (see Figs. 2 and 3). We have performed Drude fits of  $\epsilon_2$  by plotting  $(\epsilon_2 \hbar \omega)^{-1}$  versus  $(\hbar \omega)^2$  (not shown). For DyP the best fit yields an uncoupled plasma energy  $\hbar \omega_p = 2.23$  eV and an energy-independent damping  $\hbar \gamma = 0.09$  eV. Assuming an effective mass equal to the free-electron mass this plasma energy corresponds to a free-carrier concentration  $N = 3.6 \times 10^{21} \text{ cm}^{-3}$  or  $N_{\text{fu}} = 0.16$  carriers per formula unit (f.u.); i.e., 0.16 is the ratio of charge carrier density to effective mass (in units of free-electron mass). For DyBi the corresponding values are  $\hbar \omega_p = 2.3$  eV,  $\hbar \gamma = 0.12$  eV,  $N = 3.8 \times 10^{21} \text{ cm}^{-3}$ , and  $N_{\text{fu}} = 0.23/\text{f.u.}$  An independent investigation<sup>34</sup> yielded a value 0.174 for DySb. Although we do not like to put too much weight on these numbers because the exact stoichiometry of the materials is not known, they do follow the expected trends. This is that increasing covalency leads to a larger overlap of the *p* valence band and the *d* conduction band and, therefore, to a larger free-carrier concentration in these materials which are of semimetallic character. Below 0.08 eV the Drude fit deviates more and more from the  $\epsilon_2$  spectrum of DyP, indicating that the assumption of a frequency-independent damping is not valid in this spectral range. Indeed, the Drude formula with the parameters given above extrapolates to dc conductivities which are smaller by a factor of 2 than those measured directly.

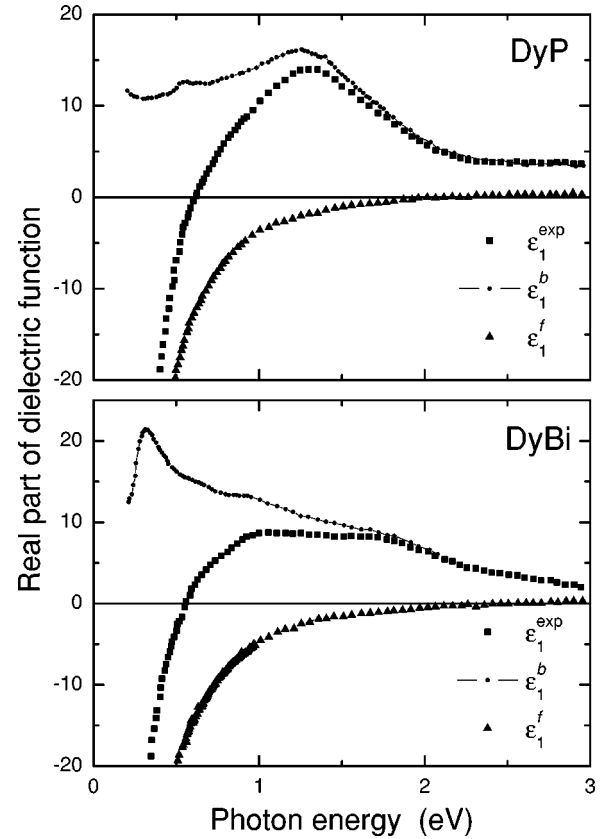
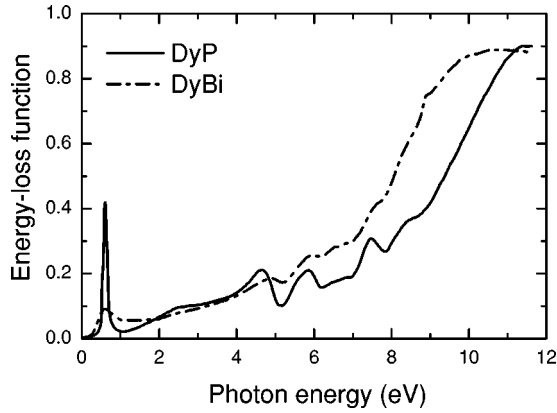


FIG. 3. Decomposition of the real part of the dielectric function ( $\epsilon_1^{\text{exp}}$ ) into the free-electron ( $\epsilon_1^f$ ) and interband ( $\epsilon_1^b$ ) contributions for DyP (top) and DyBi (bottom).

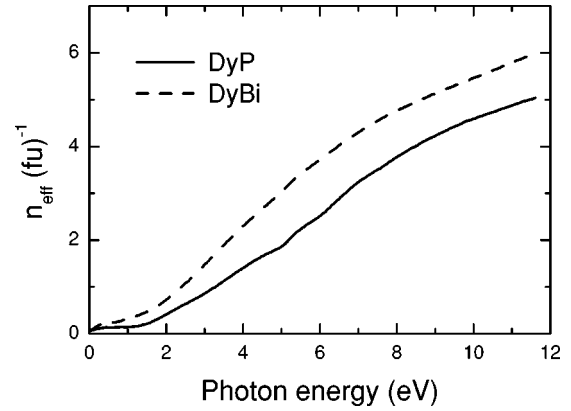
As mentioned above, the rare-earth pnictides tend to be nonstoichiometric. The nonstoichiometry can affect the magnetic and transport behavior as well as the intraband optical effects. However, the main issues of the present investigation are the interband optical effects. The calculations do not include intraband transitions and the experimental results (see, e.g., Fig. 2) show that intraband contributions are negligible above 1 eV.

To investigate the interband transitions at low energies, we have made a decomposition of the dielectric function into intraband and interband contributions. In order to do this, we start from the Drude fits and calculate the free-electron contribution to  $\epsilon_2$  which we call  $\epsilon_2^f$ . The interband contribution to  $\epsilon_2$  is obtained simply by setting  $\epsilon_2^b = \epsilon_2 - \epsilon_2^f$ . The interband contribution to  $\epsilon_1$ ,  $\epsilon_1^b$ , is obtained through a Kramers-Kronig transformation of  $\epsilon_2^b$ . (One should bear in mind that the effect of the interband transitions is much less localized in energy for  $\epsilon_1$  than for the absorptive part of the dielectric constant,  $\epsilon_2$ .) Here  $\epsilon_1^f$  can be computed either from the Drude formula or from the relation  $\epsilon_1^f = \epsilon_1 - \epsilon_1^b$ , so that the comparison of both can be used as a self-consistency check. For both compounds we obtained an agreement within a few percent. The low-energy parts of the various  $\epsilon_2$  and  $\epsilon_1$  spectra are displayed in Figs. 2 and 3, respectively.<sup>43</sup> Examining the  $\epsilon_2^b$  spectra we see that the onset of the interband transitions moves to lower energy on going from DyP to DyBi, in full agreement with the covalency trend rationale (that DyBi

FIG. 4. Energy-loss function  $\text{Im}[-\epsilon^{-1}(\omega)]$  of DyP and DyBi.

is more covalent than DyP) developed above for the free-carrier discussion. The shift of the onset of the major interband transition is from  $\cong 1$  eV in the phosphide to 0.3 eV in the bismuthide. We assign this onset of strong interband transitions to direct transitions between the valence and conduction bands. Despite the small misfit for DyP near 0.5 eV, the data for this compound clearly indicate some small interband transitions starting near 0.5 eV. The comparison of the decomposed  $\epsilon_2$  spectra for the two materials beautifully shows the much stronger overlap of intraband and interband transitions in DyBi compared to DyP. The examination of  $\epsilon_1^{\text{exp}}$  and  $\epsilon_1^f$ , as shown in Fig. 3, illustrates the dressing effect of the dielectric function originating from interband transitions on the plasma frequency of the free carriers (i.e., giving the shift downward in energy between the zero crossing of  $\epsilon_1^f$  and that of  $\epsilon_1^{\text{exp}}$ ). (The free plasmon frequency  $\omega_p$  is dressed by the dielectric function to become  $\omega_p^* = \omega_p / \sqrt{\epsilon_1}$ .) The strong peak in  $\epsilon_1^b$  of DyBi near 0.3 eV (which goes with the sharp rise of  $\epsilon_2^b$  in Fig. 2) indicates the presence of a narrow interband transition at the onset of the fundamental absorption.

Figure 4 displays the energy-loss function for the two materials. Peaks in the energy-loss function indicate either single-electron or collective mode excitations. In general, the comparison with  $\epsilon(\omega)$  or  $\sigma(\omega)$  allows us to distinguish the two types of excitations. Peaks at similar energies in  $\text{Im}[-\epsilon^{-1}]$  and  $\sigma_1$  indicate single-electron excitations and peaks in  $\text{Im}[-\epsilon^{-1}]$  at energies where  $\epsilon_1$  and  $\epsilon_2$  are small and  $d\epsilon_1/d\omega > 0$  indicate collective excitations. It follows that the peaks at 0.6 eV and 11.5 eV in DyP and 0.6 eV and 10.5 eV in DyBi correspond to collective excitations; all other peaks correspond to single-electron excitations. The low-energy collective modes are the dressed (or screened) free-carrier plasmons. The different sharpness in the two materials reflects the much larger damping in DyBi compared to DyP. The high-energy collective modes correspond to the collective excitation of the valence-band electrons. Assuming six valence electrons  $N_v$  per formula unit, the expression  $\omega_p = (4\pi N_v e^2/m)^{1/2}$  leads us to expect these valence electron plasmons to occur at 13.6 eV in DyP and at 11.7 eV in DyBi. Taking into account the uncertainty introduced by the extrapolation of the reflectivity, the agreement must be considered as good, and it corroborates the assignment.

FIG. 5. Effective number of electrons,  $n_{\text{eff}}$ , that contribute to the optical transitions up to a given photon energy for DyP and DyBi.

The last type of optical function which we want to present before discussing the theoretical results is the effective number of electrons,  $n_{\text{eff}}$ , contributing to optical transitions up to a variable energy. This integral function presents a consistency check on the assignments of optical transitions. Figure 5 shows the results for the two compounds. At low energies we find the contribution from the intraband transitions saturating near 0.15 and 0.25 carriers per formula unit in DyP and DyBi, respectively. Interband transitions set in at a lower energy in DyBi than in DyP and the anticipated six electrons per formula unit with trivalent Dy for the valence to conduction-band transitions are reached in the bismuthide near the end of the investigated spectral range, while for the phosphide nearly one electron is still lacking at 12 eV. This finding is in agreement with the estimates performed above for the valence plasmons and it indicates in what energy range transitions from the valence band are exhausted.

## B. Optical conductivity

The complex dielectric function  $\epsilon(\omega)$  is related to the optical conductivity  $\sigma(\omega)$  by  $\epsilon(\omega) = 1 + 4\pi i\sigma(\omega)/\omega$ . The optical conductivity can be computed from the energy band structure using the common linear-response expression (see, e.g., Ref. 44). The absorptive part of the interband optical conductivity is given by

$$\sigma_1(\omega) = \frac{e^2}{8m^2\pi^2\omega} \sum_{nn'} \int_{BZ} d\mathbf{k} |P_{nn'}(\mathbf{k})|^2 \delta(E_{n\mathbf{k}} - E_{n'\mathbf{k}} - \hbar\omega), \quad (1)$$

where  $E_{n\mathbf{k}}$  is the single-electron energy and  $P_{nn'}$  is the matrix element of the momentum operator,  $P_{nn'} \equiv \langle n\mathbf{k} | p | n'\mathbf{k} \rangle$ . For a cubic solid one has  $P \equiv P_x = P_y = P_z$ . The intraband or free-electron contribution to the optical conductivity can be expressed in Drude form  $\sigma^{\text{intra}}(\omega) = i\omega_p^2/[4\pi(\omega + i\tau^{-1})]$  where  $\omega_p$  is the intraband plasma frequency and  $\tau$  the relaxation time of conduction electrons. The intraband plasma frequency can be calculated from

$$\omega_p^2 = \frac{e^2}{2m^2\pi^2} \sum_n \int_{BZ} d\mathbf{k} |P_{nn}(\mathbf{k})|^2 \delta(E_{n\mathbf{k}} - E_F). \quad (2)$$

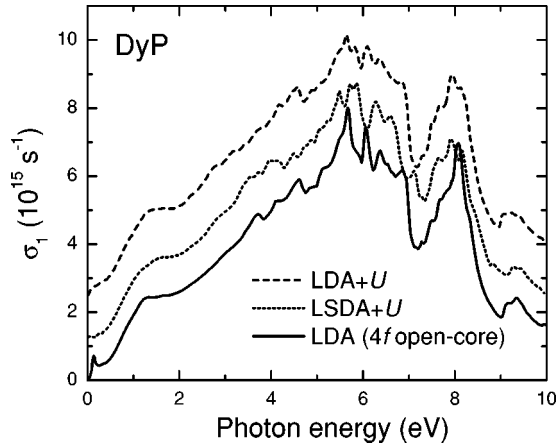


FIG. 6. The optical conductivity of DyP calculated with three different schemes to treat the  $4f$  electrons: the  $4f$  open-core,  $LDA+U$ , and  $LSDA+U$  approaches. For visibility purposes the  $LSDA+U$  and  $LDA+U$  optical conductivities have been shifted upwards by one and two units, respectively.

The  $k$ -space integration is performed by the improved tetrahedron method of Blöchl *et al.*<sup>45</sup> at 286  $k$  points in the irreducible wedge, which corresponds to 10 000 points in the whole Brillouin zone. The calculated interband optical conductivity is convoluted with a Lorentzian broadening function in order to compare with the experimental results. The width of the broadening function is set to a value of 1 mRy.

Before we proceed to compare theoretical and experimental spectra we consider the dependence of the computed spectra on the approach adopted to treat the  $4f$  electrons. Figure 6 shows the interband optical conductivity of DyP as calculated with the  $4f$  open-core, the  $LDA+U$ , and  $LSDA+U$  approaches. The differences seen between the three spectra are only modest. The main features are present in each of the spectra. Some small differences between the  $LDA+U$  and  $LSDA+U$  spectra originate from a partial spin polarization of the valence states. As mentioned before, the ferromagnetic polarization does not correspond to the experimental situation. On the other hand, the open-core calculation with no local moment present on Dy is an approximation as well. The differences in the spectra corresponding to the various treatments of the Dy  $4f$  electrons being only moderate leads us to conclude that the  $4f$  states neither affect the optical spectrum directly through interband transitions nor indirectly through spin-polarization caused by the  $4f$ 's or through hybridization with other states. In particular, we find that for the Dy monopnictides the different treatments of the  $4f$  electrons do not give rise to different spectra. In the following we shall therefore not compare the experimental spectra with results obtained by each of the different approaches, but we shall compare only to spectra obtained with the open-core approach.

We first consider the free-electron part of the spectrum. The calculated plasma energies are 2.57 eV (DyP) and 2.51 eV (DyBi), which are in fairly good agreement with the experimental values of 2.23 eV (DyP) and 2.30 eV (DyBi). The latter are obtained by fitting a Drude-form conductivity to the measured spectra.

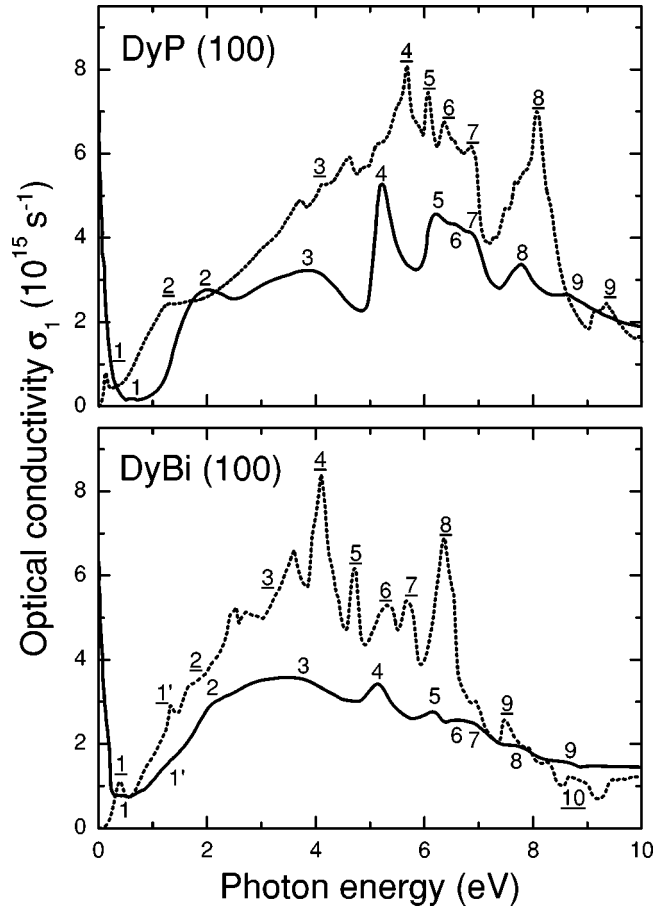


FIG. 7. Experimental and calculated optical conductivity  $\sigma_1(\omega)$  of DyP (top) and DyBi (bottom). The measured spectra are depicted by the solid curves and the calculated spectra by the dotted curves. The subsequent peaks in the measured spectra are numbered 1–9 for DyP and 1–9 and 1' for DyBi, while the peaks in the theoretical spectra are labeled  $\underline{1}$ – $\underline{9}$  and  $\underline{1}$ – $\underline{10}$  and  $\underline{1}'$  for DyP and DyBi, respectively.

The experimental and calculated optical conductivities of DyP and DyBi are shown in Fig. 7. The calculated spectra do not include the intraband effects. The free-electron contribution to the spectrum is significant — both theoretically and experimentally — only below 1 eV. It causes the sharp increase of the measured  $\sigma_1(\omega)$  below 0.5 eV which is consequently not present in the theoretical curve. The peak structures in the experimental spectra have been labeled with numbers 1–9, corresponding to the numbers given in Fig. 1 for the reflectivity spectra. For DyBi there is the additional number 1' for the weak peak at 1.3 eV. The tiny peak 1 at 0.5 eV was not numbered in the corresponding reflectivity spectrum, because there it was largely masked by the free-electron contribution. We have added numbers  $\underline{1}$ – $\underline{9}$  ( $\underline{1}$ – $\underline{10}$  and  $\underline{1}'$ , respectively) to the calculated spectra to facilitate comparison of the peak structures. Overall, the calculated and experimental spectra agree well for DyP, but less well for DyBi.

We first discuss the peak structures for DyP. The calculated small peak  $\underline{1}$  below 0.5 eV corresponds to the measured peak 1, which is barely visible as it is overwhelmed by the

strong intraband resonance. The small steplike structure 2 around 1–2 eV has almost the same shape in theory and experiment. The experimental spectrum exhibits a broad structure 3 at about 4 eV, where the calculation displays several small peaks. The prominent experimental peak 4 is given by the theory as well, but at 0.7 eV higher energy. Between 6 and 7 eV the experiment shows two peaks 5 and 7 with a tiny structure 6 in between. This part of the spectrum agrees with the theoretical spectrum, where similar peaks are found. The next peak 8 is present both in the calculation and experiment, but its intensity is stronger in the calculation. We remark that we used here only a constant Lorentzian broadening, whereas experimentally high-energy transitions are more strongly damped. Finally, there is a small peak at about 9 eV that again can be identified both in the experiment and calculation.

For DyBi we obtain a less good agreement between theory and experiment (see Fig. 7). In the experimental conductivity spectrum of DyBi weaker and broader structures are found, while the theoretical spectrum rather exhibits peaks. The first small peak 1 is present both in the calculation and experiment. The weak shoulder labeled 1' is also present in both, as is also structure 2 above 2 eV. The next measured peak 3 is rather broad and its theoretical counterpart cannot unambiguously be identified, because two peaks are placed close together in the theoretical spectrum and occur in the vicinity of 3. The same difficulty occurs for the unambiguous assignment of experimental peaks 4, 5, 6, and 7. Peak 4 lies in between the theoretical peaks  $\underline{4}$  and  $\underline{6}$ , whereas structure 5 lies in between  $\underline{5}$  and  $\underline{8}$ . Thus, the experimental and theoretical  $\sigma_1(\omega)$  of DyBi correspond for photon energies below 4 eV, but for higher energies there are deviations.

### C. Energy band structure and DOS

The interband contributions to the spectrum can be related to the band structure in terms of band-to-band optical transitions. The relativistic energy band structures of DyP and DyBi, calculated with the open-core approach at the experimental lattice constants along major symmetry directions of the Brillouin zone, are shown in Figs. 8 and 9, respectively. To make a discussion of the interband transitions easier, we have numbered the bands with increasing energy from 1 to 9. Although the band structures of DyP and DyBi are similar, they are not identical, particularly due to the large spin-orbit splitting of  $p$  states of bismuth. This splitting is visible at the  $\Gamma$  point as the splitting between band 1 and the bands 2 and 3. For DyP, band 1 is partially occupied, while it is fully occupied and completely separated from bands 2 and 3 for DyBi. The three bands are derived from the pnictogen  $p$  bands (see the discussion of the DOS below), which hybridize with the Dy  $d$  bands, located above  $E_F$ . These unoccupied bands move, for DyBi, about 1 eV downward relative to the Fermi energy. A clear hybridization of the pnictogen  $p$  and Dy  $5d$  states can be recognized for band 4, which crosses the Fermi level at the middle point of the  $\Delta$  axis for both DyP and DyBi.

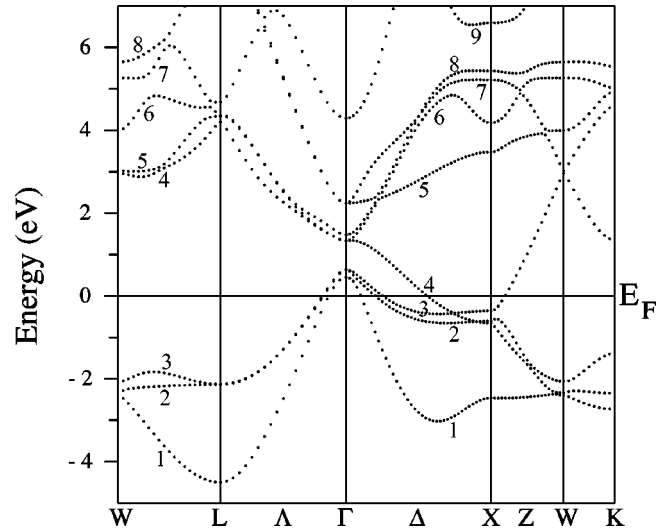


FIG. 8. Energy band structure of DyP along the major symmetry directions of the fcc Brillouin zone. The open-core approach to the  $4f$  states was used.

The total and angular momentum decomposed densities of states (DOS) are shown in Fig. 10. The bands arising from Dy  $5p$  and  $5s$  states located at about  $-22$  eV and  $-10$  eV below  $E_F$  are not shown. The two sharp peaks around  $-2$  eV are due to the pnictogen  $p$  states, as is also the broader peak at about  $-3$  eV. At the Fermi energy, the DOS is very small and exhibits a broad minimum. The width of the shallow minimum decreases with the increase of the pnictogen atomic number. The width of the bands below  $E_F$  and the DOS at  $E_F$  do almost not vary with the pnictogen atom. The peaks above  $E_F$  are mainly derived from the Dy  $d$  states. The partial DOS exemplifies that the dominant hybridization occurs among  $p$  (P, Bi) and  $d$  (Dy) states: the Dy  $d$  DOS follows closely the shape of the pnictogen  $p$  partial DOS around  $-2$  eV below  $E_F$ . Above  $E_F$ , the hybridization is seen as the shallow tail of the pnictogen  $p$  DOS, which extends over the whole range of the Dy  $d$  states. In the case of DyBi, there

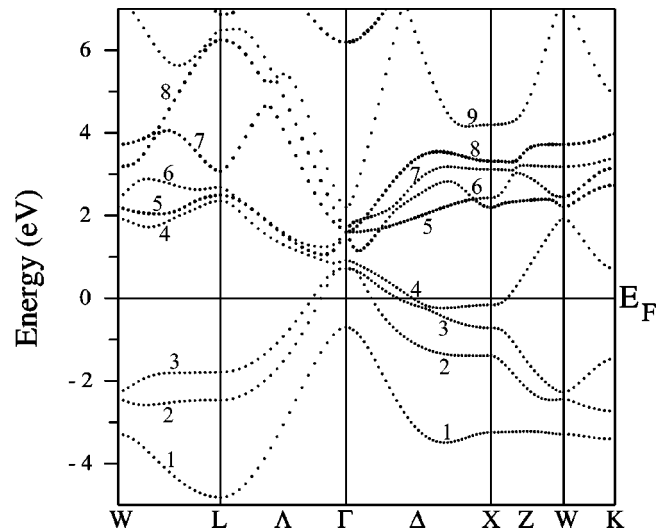


FIG. 9. As Fig. 8, but for DyBi.

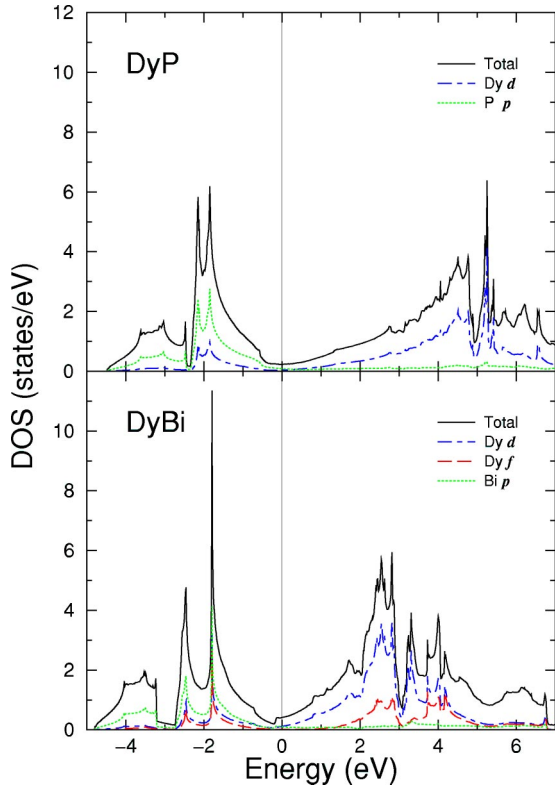


FIG. 10. (Color online) The total and partial density of states (DOS) of DyP (top) and DyBi (bottom).

is also a small contribution of the (unoccupied) Dy  $4f$  states, which hybridize with the Dy  $d$  states and with the Bi  $p$  states. The contribution of the Dy  $f$  DOS is so small for DyP that it has not been included in the plot. The partial DOS shows that the occupied bands 1, 2, and 3 and unoccupied bands 4–8 possess primarily pnictide  $p$  character and Dy  $d$  character, respectively. Taking the dipole selection rule  $\Delta l = \pm 1$  into account, a main outcome of the partial DOS is that all the interband peaks are mostly due to transitions from occupied  $p$  states of P (Bi) to unoccupied Dy  $d$  states and from occupied Dy  $d$  states to unoccupied  $p$  or  $f$  states. In particular, the combination of sharply peaked resonances in the DOS of DyP at  $-2$  eV and above 5 eV would produce a sizable peak at about 8 eV in the optical conductivity. For the bismuthide one expects a peak at a lower energy, because the unoccupied bands are closer to the Fermi energy.

#### D. Analysis of the optical conductivity

To substantiate the origin of the various peaks in the spectra we have made a decomposition of the interband conductivity spectrum into band-by-band contributions. These individual band-by-band conductivity spectra are shown in Figs. 11 and 12 for DyP and DyBi, respectively. The numbers that indicate the peak structures correspond to the numbering of the bands given in Figs. 8 and 9; i.e., 3–5 denotes transitions from band 3 to band 5. The band-by-band decomposition demonstrates that the small feature **1** at about 0.5 eV for DyP (see Fig. 7) is due transitions from band 1 to bands 2 and 3 along the  $\Delta$  axis. The next feature in the spectrum, **2**, which

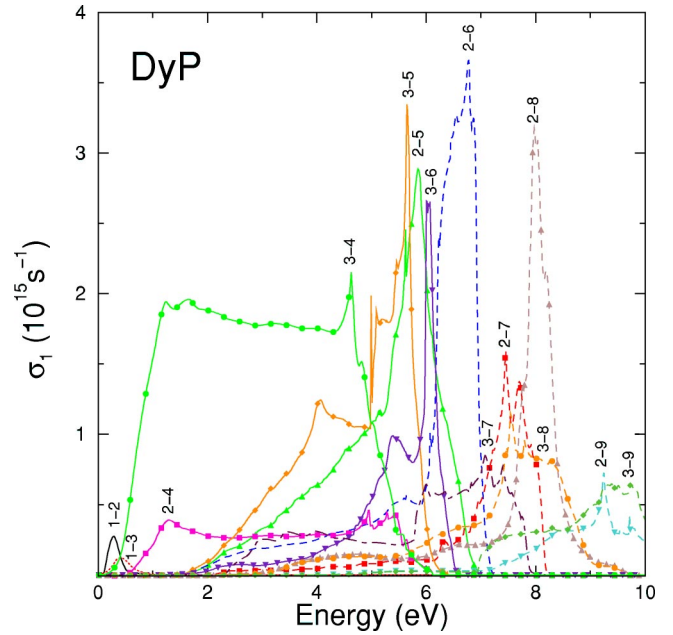


FIG. 11. (Color online) Band-by-band decomposition of the interband optical conductivity  $\sigma_1(\omega)$  of DyP. The numbers give the initial and final bands out of which the spectrum arises.

is much more pronounced, stems from transitions of bands 2 and 3 to band 4 along  $\Gamma$ -X. Here strong  $p$  to  $d$  transitions set in above 1 eV. The next peak **3**, which actually is a superposition of three small peaks, is mainly due to transitions of band 3 to bands 4 and 5. The small peaks in **3** originate from transitions along  $W$ -L,  $L$ - $\Gamma$ , and  $\Gamma$ -X. Also transitions from band 2 to bands 4 and 5 contribute to the total intensity. For example, bands 3 and 4 are rather flat and parallel along

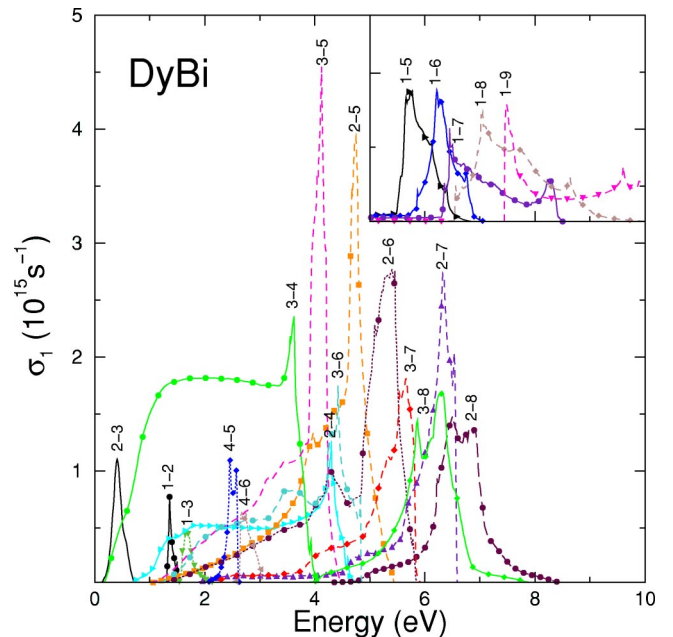


FIG. 12. (Color online) As Fig. 11, but for DyBi. For sake of visibility, several of the band-by-band decomposed optical conductivities are shown in the inset.

$W-L$ , giving rise to the peak at 4.5 eV. Also along  $W-L$  bands 2 and 3 are quasiparallel to band 5, leading to the peaks denoted  $\underline{4}$  and  $\underline{5}$ . The next higher in energy structure is built up of two small peaks  $\underline{6}$  and  $\underline{7}$  stemming from transitions of band 2 to band 6, taking place again mainly along  $W-L$ . Peak  $\underline{8}$ , likewise, consists of a dominant peak with small shoulders, which are due to excitations from bands 2 and 3 to bands 7 and 8, taking place along the  $W-L$  section. The strongest contribution is given by transitions from band 2 to 8. The last small structure  $\underline{9}$  can be identified to result from excitations of bands 2 and 3 to band 9.

An analogous analysis can be carried through for DyBi. On account of the large spin-orbit splitting at the  $\Gamma$  point band 1 is now completely occupied, which implies readily that band 1 will contribute more to the spectrum of DyBi. The peak  $\underline{1}$  at 0.5 eV is now due to transitions between bands 2 and 3 in the neighborhood of the  $\Gamma$  point. The transitions of band 1 to bands 2 and 3 give rise to the small structure  $\underline{1}'$  at 1.3 eV in the calculated spectrum, which is present in the measured spectrum as well (see Fig. 7). The smooth step  $\underline{2}$  in the theoretical spectrum, which sets in above 1 eV, is due to transitions along  $L-\Gamma$  from bands 2 and 3 to 4, just as in case of DyP. The next structure, to the left of  $\underline{3}$ , originates from transitions near the  $X$  point from band 4 to bands 5 and 6. Also the origin of the peak  $\underline{4}$  at 4 eV is the same as peak  $\underline{4}$  in DyP: transitions from band 3 to band 5, mainly along  $W-L$ . Peak  $\underline{5}$  is mainly due to bands 2 and 5, which are quasiparallel along  $W-L$ . The next peak structures labeled  $\underline{6}$ ,  $\underline{7}$ , and  $\underline{8}$  can be seen to originate from excitations of band 2 to bands 6, 7, and 8 and of band 3 to 7 and to 8. In addition contributions from bands 1 to 5 and 6 appear, which played no role for DyP. Also, peak  $\underline{9}$  and the small hump  $\underline{10}$  at about 9 eV are brought about by transitions of band 1 to bands 7, 8, and 9, along  $W-L$  and  $\Gamma-X$ .

The differences between the calculated optical spectra of DyP and DyBi thus can be understood to follow from the modification of the energy bands by the larger spin-orbit interaction on Bi and from an overall shift of the hybridized Dy  $d$  bands towards the Fermi level for the bismuthide. This shift of the  $d$  bands places some of the peaks at lower photon energies for DyBi (see, e.g., the contributions to both peaks labeled  $\underline{4}$  from band 3 to 5 in Figs. 8 and 9). Furthermore, transitions from the spin-orbit split initial band 1 give rise to additional structures, such as, e.g., peak  $\underline{1}'$  at 1.3 eV.

For sake of completeness of our study of the dysprosium monpnictides we have also calculated the optical conductivity spectra of DyAs and DySb, employing the open-core approach. These spectra, calculated for the experimental lattice constants, are given in Fig. 13. The labeling of the peaks corresponds to that introduced for DyP, with the exception of the small peak  $\underline{6}$ , which cannot unambiguously be identified. From these spectra one can observe characteristic changes in the optical spectrum of the Dy monpnictides when the pnictide series is traversed. These characteristic changes are due to the increase of the lattice parameter with the pnictogen atomic number and the variation of the pnictogen  $p$  band. The overlap of the pnictide  $p$  states and the Dy  $d$  states decreases due to the increase of the lattice constant from 5.63 Å for DyP to 6.24 Å for DyBi. Figure 13 illustrates that the

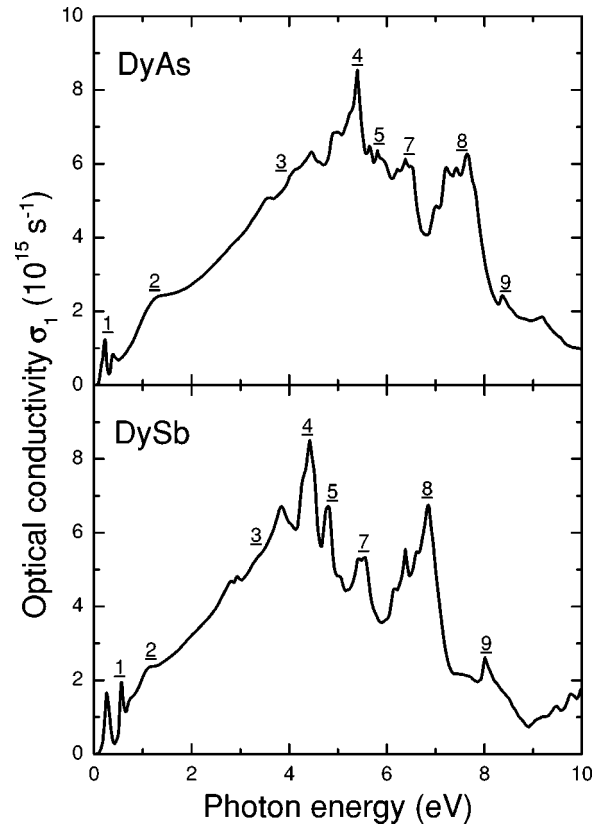


FIG. 13. Real part of the interband optical conductivity  $\sigma_1(\omega)$  of DyAs and DySb, computed using the open-core approach to the Dy  $4f$  electrons.

spectrum of DyAs is rather similar to that of DyP while that of DySb approaches that of DyBi. The increase of the spin-orbit coupling leads to a splitting of the small peak  $\underline{1}$  for DyP into a double peak for DyAs and DySb, which consistently splits more for DyBi, where the higher-energy part merges with the steplike shoulder to form peak  $\underline{1}'$  of DyBi. The single peak  $\underline{4}$  in DyP gradually splits for DyAs and DySb and further for DyBi. The shift of the Dy  $d$  band towards the Fermi energy with the increase of the pnictogen atomic number causes the gradual shift of peak  $\underline{4}$  from 5.5 eV for DyP to 4 eV for DyBi and of peak  $\underline{8}$  from 8 eV for DyP to 6.5 eV for DyBi. These changes in the spectra can consequently be understood from the changes of the energy band structure within the Dy pnictide series.

## V. CONCLUSIONS

The electronic and optical properties of the dysprosium monpnictides have been studied systematically. Optical experiments were carried out on single crystals of DyP and DyBi—in part under ultrahigh-vacuum and in part under high-vacuum conditions—in the energy range of 0.03–12 eV. From these measurements the complex dielectric function, the energy-loss function, the effective number of electrons, and the optical conductivity were derived.

The Dy monpnictides are found to be poor metals, as follows from the small number of free carriers per formula

unit, of 0.16 and 0.23, for DyP and DyBi, respectively. This finding is consistent with the calculated low DOS at the Fermi energy, suggesting semimetallic behavior. It is also consistent with the calculated plasma frequencies, which relate to the number of free carriers, which are very close to the measured plasma frequencies.

The experimental results for the optical conductivity are compared to *ab initio* theoretical spectra that were obtained using the FLAPW band structure method. To investigate what is the most appropriate treatment of the Dy  $4f$  electrons, we have carried out calculations with the  $4f$  open-core approach and with the LDA+ $U$  as well as the LSDA+ $U$  approach. For the Dy monpnictides these three approaches to treat the  $4f$  states lead to rather similar results for the *optical conductivity*. The good agreement between the experimental and theoretical conductivity spectra of DyP prompts the conclusion that the electronic structure of DyP is well captured by the open-core approach. Almost all the peaks and shoulders in the measured conductivity spectrum can be attributed to specific band-by-band optical transitions. The measured optical conductivity of DyBi compares reasonably with the theoretical open-core spectrum up to 4 eV, but at higher energies the agreement is less good. The differences in the peak heights and peak positions that exist between theory and experiment do not appear to rest in aspects

of the treatment of the  $4f$  states, but rather to be due to shortcomings in the description of the valence-band states. The energy positions of the computed valence bands, as well as their energy dispersions, differ somewhat from the real bands, leading to the mentioned discrepancies in the peak positions and heights. The conductivity spectra of the dysprosium monpnictides displays several typical changes with increasing pnictogen atomic number. The increasing spin-orbit coupling splits the  $p$  bands farther, giving rise to the occurrence of related spectral structures. Furthermore, the Dy  $d$  band shifts more towards the Fermi energy for the heavier pnictides, which causes a shift of peaks to lower photon energies.

The overall good agreement between experimental and theoretical optical data establishes that the Dy  $4f$  electrons do not play an active role in the bonding properties of trivalent dysprosium monpnictides.

#### ACKNOWLEDGMENTS

This work is funded under the exchange program between the Department of Science and Technology (DST, No. INT/DST/DAAD/P-49/2001), Government of India, and the German DAAD (DAAD No. 0026524), and by the German Sonderforschungsbereich 463, Dresden.

- 
- <sup>1</sup>J. Rosat-Mignod, J. M. Effantin, P. Burlet, T. Chattopadhyay, L. P. Regnault, H. Bartholin, C. Vettier, O. Vogt, D. Ravot, and J. C. Achart, *J. Magn. Magn. Mater.* **52**, 111 (1985).
- <sup>2</sup>T. Chattopadhyay, P. Burlet, J. Rosat-Mignod, H. Bartholin, C. Vettier, and O. Vogt, *Phys. Rev. B* **49**, 15 096 (1994).
- <sup>3</sup>R. Pittini, J. Schoenes, O. Vogt, and P. Wachter, *Phys. Rev. Lett.* **77**, 944 (1996).
- <sup>4</sup>R. Pittini, J. Schoenes, F. Hulliger, and P. Wachter, *Phys. Rev. Lett.* **76**, 3428 (1996).
- <sup>5</sup>O. Vogt and K. Mattenberger, *Physica B* **215**, 22 (1995).
- <sup>6</sup>P. Wachter, E. Kaldis, and R. Hauger, *Phys. Rev. Lett.* **40**, 1404 (1978).
- <sup>7</sup>J. Schoenes, H. Brändle, A. Weber, and F. Hulliger, *Physica B* **163**, 496 (1990).
- <sup>8</sup>Y. S. Kwon, M. Takeshige, O. Nakamura, T. Suzuki, and T. Kasuya, *Physica B* **171**, 316 (1991).
- <sup>9</sup>Y.-S. Kwon, T. Suzuki, and T. Kasuya, *Jpn. J. Appl. Phys. Ser. 8*, 104 (1993).
- <sup>10</sup>S. Kimura, F. Arai, Y. Haga, T. Suzuki, and M. Ikezawa, *Physica B* **206–207**, 780 (1995).
- <sup>11</sup>F. Salghetti-Drioli, P. Wachter, and L. Degiorgi, *Solid State Commun.* **109**, 773 (1999).
- <sup>12</sup>S. Kimura, H. Kitazawa, G. Kido, and T. Suzuki, *J. Phys. Soc. Jpn.* **69**, 647 (2000).
- <sup>13</sup>T. Kasuya, O. Sakai, J. Tanaka, H. Kitazawa, and T. Suzuki, *J. Magn. Magn. Mater.* **63 & 64**, 64 (1987).
- <sup>14</sup>K. Morita, T. Goto, H. Matsui, S. Nakamura, Y. Haga, T. Suzuki, and M. Kataoka, *Physica B* **206 & 207**, 795 (1995).
- <sup>15</sup>Y. Nakanishi, F. Takahashi, T. Sakon, M. Yoshida, D. X. Li, T. Suzuki, and M. Motokawa, *Physica B* **281 & 282**, 750 (2000).
- <sup>16</sup>A. Delin, P. M. Oppeneer, M. S. S. Brooks, T. Kraft, B. Johansson, and O. Eriksson, *Phys. Rev. B* **55**, R10 173 (1997).
- <sup>17</sup>J. Schoenes, in *Moment Formation in Solids*, edited by W. J. L. Buyers (Plenum, New York, 1984), p. 237.
- <sup>18</sup>H. Kumigashira, S.-H. Yang, T. Yokoya, A. Chainani, T. Takahashi, A. Uesawa, and T. Suzuki, *Phys. Rev. B* **55**, R3355 (1997).
- <sup>19</sup>P. Wachter, in *Handbook on the Physics and Chemistry of Rare Earths*, edited by K. A. Gschneidner, Jr., L. Eyring, G. H. Lander, and G. R. Choppin (North-Holland, Amsterdam, 1994), Vol. 19, p. 132.
- <sup>20</sup>M. S. S. Brooks and B. Johansson, in *Handbook of Magnetic Materials*, edited by K. H. J. Buschow (North-Holland, Amsterdam, 1993), Vol. 7, p. 139.
- <sup>21</sup>R. Ahuja, S. Auluck, B. Johansson, and M. S. S. Brooks, *Phys. Rev. B* **50**, 5147 (1994).
- <sup>22</sup>A. G. Petukhov, W. R. L. Lambrecht, and B. Segall, *Phys. Rev. B* **53**, 4324 (1996).
- <sup>23</sup>V. I. Anisimov, J. Zaanen, and O. K. Andersen, *Phys. Rev. B* **44**, 943 (1991).
- <sup>24</sup>V. I. Anisimov, I. V. Solovyev, M. A. Korotin, M. T. Czyzyk, and G. A. Sawatzky, *Phys. Rev. B* **48**, 16 929 (1993).
- <sup>25</sup>M. T. Czyzyk and G. A. Sawatzky, *Phys. Rev. B* **49**, 14 211 (1994).
- <sup>26</sup>A. I. Liechtenstein, V. I. Anisimov, and J. Zaanen, *Phys. Rev. B* **52**, R5467 (1995).
- <sup>27</sup>A. I. Liechtenstein, V. P. Antropov, and B. N. Harmon, *Phys. Rev. B* **49**, 10 770 (1994).
- <sup>28</sup>B. R. Cooper, S. P. Lim, I. Avgin, Q. G. Sheng, and D. L. Price, *J. Phys. Chem. Solids* **56**, 1509 (1995).
- <sup>29</sup>A. N. Yaresko, P. M. Oppeneer, A. Y. Perlov, V. N. Antonov, T.

- Kraft, and H. Eschrig, *Europhys. Lett.* **36**, 551 (1996).
- <sup>30</sup>M. De and S. K. De, *J. Phys.: Condens. Matter* **11**, 6277 (1999).
- <sup>31</sup>D. B. Ghosh, M. De, and S. K. De, *Phys. Rev. B* **67**, 035118 (2003).
- <sup>32</sup>A. Svane, Z. Szotek, W. M. Temmerman, and H. Winter, *Solid State Commun.* **102**, 473 (1997).
- <sup>33</sup>J. Schoenes, P. Repond, F. Hulliger, S. P. Lim, and B. R. Cooper, *J. Magn. Magn. Mater.* **177–181**, 1046 (1998).
- <sup>34</sup>Y. S. Kwon, M. H. Jung, K. R. Lee, S. Kimura, and T. Suzuki, *Physica B* **240**, 88 (1997).
- <sup>35</sup>J. Schoenes, *Phys. Rep.* **66**, 187 (1980).
- <sup>36</sup>P. Blaha, K. Schwarz, and J. Luitz, computer code WIEN 2K FLAPW code, Vienna University of Technology, Vienna, 2000.
- <sup>37</sup>J. P. Perdew and Y. Wang, *Phys. Rev. B* **45**, 13 244 (1992).
- <sup>38</sup>J. Kuneš, P. Novák, M. Diviš, and P. M. Oppeneer, *Phys. Rev. B* **63**, 205111 (2001).
- <sup>39</sup>A. B. Shick, W. E. Pickett, and C. S. Fadley, *Phys. Rev. B* **61**, R9213 (2000).
- <sup>40</sup>G. Güntherodt, E. Kaldis, and P. Wachter, *Solid State Commun.* **15**, 1435 (1974).
- <sup>41</sup>Y. S. Kwon, M. Takeshige, T. Suzuki, and T. Kasuya, *Physica B* **163**, 328 (1990).
- <sup>42</sup>A. Schlegel, Ph.D. thesis, ETH Zürich, 1979.
- <sup>43</sup>We have additional data to lower energies than that shown for DyBi (namely, down to 0.03 eV). The decomposition into interband and intraband contributions has been made by plotting  $(\epsilon_2 \hbar \omega)^{-1}$  versus  $(\hbar \omega)^2$  and not from Fig. 2, which shows only the result of the decomposition.
- <sup>44</sup>J. Callaway, *Quantum Theory of Solids* (Academic, New York, 1974).
- <sup>45</sup>P. E. Blöchl, O. Jepsen, and O. K. Andersen, *Phys. Rev. B* **49**, 16 223 (1994).